Journal homepage: http://revues.imist.ma/?journal=jasi

ISSN: 2550-4800

https://doi.org/10.48442/IMIST.PRSM/jasi-v3i1-3.11215

Synthesis, structural and vibrational studies of lacunar apatite type $NaPb_2CaSr(PO_4)_3$ and application to phosphoric acid demetallization

S. Louihi [1], M. Azdouz [2], Z. Chchiyai [1], B. Manoun [1,3,], Y. Tamraoui [1,3], A. Nia [4], E. Magha [4], J. Biya [4], P. Lazor [5].*

[1] *Univ. Hassan 1er, Laboratoire des Sciences des Matériaux, des Milieux et de la modélisation (LS3M), 25000, Khouribga, Morocco.*
[2] *Laboratoire de Physico-Chimie des Matériaux, Département de Chimie, FST Errachidia, Morocco.*
[3] *Materials Science and Nano-engineering Department, University Mohammed VI Polytechnic, Ben Guerir, Morocco.*
[4] *Laboratoire Central OIS/L/Q de Maroc Chimie, Safi, Morocco.*
[5] *Department of Earth Sciences, Uppsala University, SE-752 36, Uppsala, Sweden.*

Received 22 January 2018; Revised 24 May 2018; Accepted 26 May 2018.

Abstract: *$NaPb_2CaSr(PO_4)_3$ lacunar apatite was synthesized by the solid-state reaction method. The compound was characterized by X-ray diffraction, Raman and infrared spectroscopies. The crystal structure of this new compound has been determined by Rietveld method, adopting the space group $P6_3/m$ (No. 176), with a = b = 9.6684(3) Å and c = 7.1104(3) Å. The analysis shows that the M(2) sites are shared by four cations Ca, Sr, Pb and Na. While the M(1) sites are occupied by the Ca, Sr and Pb cations. The structure was described as built up from $[PO_4]^{3-}$ tetrahedra and $Pb^{2+}/Ca^{2+}/Sr^{2+}$ of six fold coordination cavities (6h positions), which delimit void hexagonal tunnels running along [0 0 1]. The tunnels are connected by cations of mixed sites (4f) half occupied by $Pb^{2+}/Ca^{2+}/Sr^{2+}$ and half by Na^+ mixed alkali cation. The results of vibrational spectroscopy are in good agreements with the XRD measurements, the assignments of internal modes of $(PO_4)^{3-}$ tetrahedra have been made and corroborate well with factor group analysis for the symmetry $P6_3/m$. An attempt to purify phosphoric acid is done using our apatite and the results are promising.*

Keywords: *Lacunar apatite; X-ray diffraction; Rietveld method; Raman spectroscopy.*

1. Introduction

Apatites have the general formula, $M_{10}(XO_4)_6Y_2$, a key feature of this structure is its ability to form solid solutions and to accept a large number of elements. where M: Ca^{2+}, Sr^{2+}, Cd^{2+}, Pb^{2+},.... ; X: P^{5+}, V^{5+}, Si^{4+}, As^{5+},...; and Y^-: F^-, OH^-, Cl^-,.....etc., form a large family of solid compounds, which crystallize, generally, in a hexagonal system with space group $P6_3/m$ [1-8]. M^{2+} denotes a divalent cation being divided into two different sites: M (1) and M (2) residing in two nonequivalent sites 6h and 4f respectively, (XO_4^{3-}) an anion usually trivalent. The only system in which compounds could be prepared with the apatite structure and without the Y anion was the lead system [9-11]. Lead is known as a 'bone seeker', it accumulates in bone and tooth mineral. As well as, it may contribute to nonstoichiometry of apatites.

Apatites with vacancies in Y^- anion sites have the general formula $APb_4(XO_4)_3$ A^+: Na^+, K^+,.....; monovalent cation, they have been studied by several authors [7,9]. It appears that the Pb^{2+} ions play an essential role to maintain the ideal apatititic network. This role is linked to the presence of electron pairs $6s^2$ that can offset the imbalance Coulomb due to the existence of anion vacancies in the tunnels apatite [12-13]. Lead-phosphorus apatite with mixed divalent and monovalent cations without Y anions $APb_{4-z}M_z(PO_4)_3\square Y_0$, caught our particular attention. Indeed, various applications have been recently experienced [14-17]. The main purpose of this work is to report on the crystal structure and vibrational spectroscopy of a new lacunar apatite type $NaPb_2SrCa(PO_4)_3$.

2. Experimental

2.1. Solid-state synthesis

The synthesis is carried out starting with the following products: PbO, Na_2CO_3, $SrCO_3$, $Ca(OH)_2$ and $(NH_4)_2HPO_4$. These products, commercial grade reagents were mixed in the amount necessary to the following reaction:

$$\tfrac{1}{2}\,Na_2CO_3 + Ca(OH)_2 + SrCO_3 + 2PbO + 3(NH_4)_2HPO_4 \xrightarrow[700°C]{\text{In air}} NaPb_2CaSr(PO_4)_3 + 1.5CO_2 + 6NH_3 + 5.5H_2O$$

The mixture was ground in an agate mortar and placed in alumina crucibles and treated progressively up to 500°C in order to improve the homogeneity of the mixture and increase the kinetics of the solid state reaction. The resulting powders were reground and calcined at 700°C for 48h. After each thermal treatment, the products were quenched to room temperature. The initial structural identification and characterization of the samples was carried out by laboratory X-ray powder diffraction ($\lambda_{Cuk\alpha}$=1.5406Å).

* *Corresponding author: E-mail: manounb@gmail.com (Bouchaib MANOUN)*

2.1. Instrumental methods

2.2.1. X-ray diffraction

The final product of $NaPb_2CaSr(PO_4)_3$ have been monitored by X-ray powder diffraction analysis using $Cu_{K\alpha}$ radiation, Fig.1. The structural refinements were undertaken from the powder data. Diffraction data were collected at room temperature on a D2 PHASER diffractometer, with the Bragg–Brentano geometry, using CuKα radiation (λ=1.5418 Å) with 30kV and 10 mA. The XRD patterns were scanned through 2θ range 10–100° with step size of 0.01° with a fixed-time counting of 10s. Rietveld's profile analysis method was employed for refinements using the FULLPROF program [18].

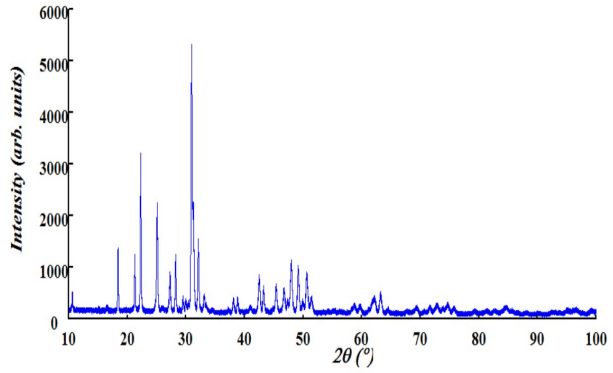

Fig.1. *X-ray powder diffraction pattern for $NaPb_2CaSr(PO_4)_3$*

2.2.2. Raman spectroscopy

Raman spectroscopy measurement was carried out in the Department of Earth Sciences, Uppsala University [10, 19]. The key system components include a high-throughput, single stage imaging spectrometer (HoloSpec f/1.8i, Kaiser Optical Systems, Inc.) equipped with a holographic transmission grating and thermoelectrically cooled two dimensional multichannel CCD detector (Newton, Andor Technology, 1600×400 pixels, thermoelectrically cooled down to -60 °C), an argon–ion laser (Spectra-Physics, 514.5 nm, 20 mW), and an optical imaging system (magnification 20×, spatial resolution ~1 µm). Two holographic notch filters (Kaiser Optical Systems, Inc.) blocked the Rayleigh line. The spectrometer was calibrated by fluorescence lines of a neon lamp. Non-polarized Raman spectra were collected in the back-scattering geometry, in the range of 180–2280 cm^{-1}, at a resolution of about 3 cm^{-1}. Accuracy and precision of spectral measurements, as estimated from the wavelength calibration procedure and peak fitting results, were 1.5 and 0.1–0.4 cm^{-1}, respectively. The acquisition time is 60s.

2.2.3. Infrared Spectra

The infrared spectrum in the spectral range between 2000 and 400 cm^{-1} was recorded using a type SP-FTIR spectrometer (The Fourier transform infrared spectroscopy), using KBr (mid-IR) pellets.

3. Refinement of the structure and discussion

3.1. Refinement of the structure

The resulting X-ray powder diffraction (XRPD) pattern for $NaPb_2CaSr(PO_4)_3$ was performed by means of the computer program DICVOL [20]. The first 37 peak positions, with a maximal absolute error of 0.03°, were used as input data. The X-ray diffraction pattern was assigned to a hexagonal apatite structure. The full pattern refinement was carried out by means of the Rietveld method using the Fullprof program integrated in WINPLOTR software [21]. The atomic coordinates of $NaPb_3Ca(PO_4)_3$ [22] with space group $P6_3/m$ were used as a starting model for Rietveld refinement. The background was adjusted with 34 variables (structural and non-structural parameters). The refinement involved 17 atomic parameters (including positions, occupancies and isotropic thermal displacements), 1 scale factor, 1 zero point, 6 background coefficients, 2 cell parameters, 2 line asymmetry parameters, using a pseudo-voigt function, 3 halfwidth parameters (these halfwidth of the diffraction peaks as a function of 2θ was evaluated by the Caglioti equation [23]). In addition, one preferred orientation parameter was refined in the direction of the diffraction vector perpendicular to (0 0 1), the results are shown in Table.1.

The final refinements, the refined lattice constants, the atomic coordinates, site occupancy, the thermal displacement parameters and their estimated standard deviations in parentheses for $NaPb_2CaSr(PO_4)_3$ are shown in Table.2, list of selected bond lengths and angles is given in Table.3.

3.2. Discussion

Rietveld first refinements plot of $NaPb_2CaSr(PO_4)_3$, showed that all the reflections could be indexed in the spatial group $P6_3/m$ (n°. 176), except for two reflections indicated at 2θ successively (29.37: 29.48) and (32.99: 33.11) with low intensity, indicated by arrows in Fig.1. The additional peaks have been detected by HighScore program [24], they were assigned to the compound $Pb_3(PO_4)_2$ [25]. At this stage of the refinements the structural model indicators converged to R_B = 10.2 % and R_F = 6.18% (Table.1).

The second refinement of the two phases is illustrated in Fig.2. The indicators of the quality of the structural model for $NaPb_2CaSr(PO_4)_3$ carried out in the $P6_3/m$ space group, converge towards R_B = 4.75% and R_F = 2.33% (Table.1), displays the agreement obtained between observed and calculated diffraction profiles. It should be noted that the refinements of $NaPb_2CaSr(PO_4)_3$ show that there are two symmetrically non-equivalent M(1) and M(2) sites, residing respectively in two sites 6h and 4f.

The structure can be described as a built up from $[PO_4]^{3-}$ tetrahedral, M(1) of six fold coordination cavities and M(2) of nine fold coordination cavities, According to the stoichiometric coefficients the formula is

$(Pb_{0.1}Ca_{0.65}Sr_{0.25}Na)(Pb_{1.9}Ca_{0.35}Sr_{0.75})[PO_4]_3$, It was noted that of 95% of Pb^{2+}, 35% of Ca^{2+} and 75% of Sr^{2+} cations are located in the 6h positions M(1), which delimit void hexagonal tunnels running along [0 0 1]. These tunnels are connected by M(2) cations of mixed sites (4f) half occupied by the rest of 5% of Pb^{2+}, 65% of Ca^{2+} and 25% of Sr^{2+} divalent cations, and half by Na^{+} alkali monovalent cations. The existence of this type of lacunar apatite is conditioned by the presence of lone pair cations Pb^{2+}, the formulation of the compound could be written as $Na_2Pb_4Ca_2Sr_2(PO_4)_6Y_2$ with Y a vacant site of the usual monovalent anions that exist in non lacunar apatites. This stabilization is interpreted by the orientation of the lone pairs $6s^2$ within the tunnels. El Koumiri et al [7], Manoun et al. [9-11], showed previously that while Pb^{2+} cations with an active lone pairs $6s^2$ are engaged in an almost ionic bond. The interatomic distances are reasonable and were determined for $(Pb^{2+}/Ca^{2+}/Sr^{2+}/Na^{+})$ – O in the mixed site M(4f), the distances vary from 2.47 to 2.75 Å. In *6h* sites, the M–O distances vary from 2.34 to 2.93 Å, $(Pb^{2+}/Ca^{2+}/Sr^{2+})$ – O is more covalent in character and the $6s^2$ lone pair of Pb^{2+} is active. P–O are with an average value of 1.579Å and the O–P–O angles are between 108.2° and 109.5°. The average distances are similar and agree well with those found in the literature. Note that the presence of lone pair electrons can distort the oxygen polyhedra, and this explain clearly our X-ray results where the M(1)–O in the mixed site M(6h) distances (Tables 2 and 3, Fig.4).

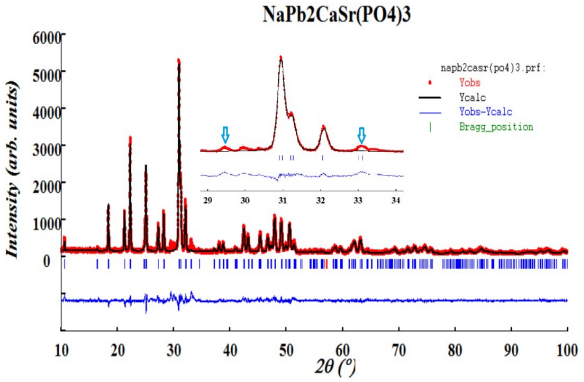

Fig.2. *Rietveld first refinements plot of $NaPb_2CaSr(PO_4)_3$. The upper symbols illustrate the observed data and the calculated pattern (solid line). The vertical markers show calculated positions of Bragg reflexions (R_{Bragg} = 10.2%). The lower curve is the difference diagram.*

Table 1
Refinement details.

		1st Refinements	*2nd Refinements*	
		$NaPb_2CaSr(PO_4)_3$	***$NaPb_2CaSr(PO_4)_3$***	***$Pb_3(PO_4)_2$***
Zero point(deg,2ϑ)		*0.0398(45)*	*0.0280(19)*	
Pseudo-Voigt function PV=ηL+(1-η)G	*η*	*0.364(11)*	*0.448(10)*	
Caglioti parameters	*U*	*0.299(23)*	*0.517(20)*	
	V	*0.049(13)*	*-0.058(12)*	
	W	*0.003(2)*	*0.016(2)*	
No of reflections		*476*	*478*	*558*
No of refined parameter		*33*	*37*	
Space group		*P 6_3/m*		*C 2/c*
a (Å)		*9.6692(5)*	*9.6684(3)*	*13.871(2)*
b (Å)				*5.6786(5)*
c (Å)		*7.1142(4)*	*7.1105(3)*	*9.265(1)*
Beta				*101.99(1)*
V (Å^3)		*576.01(5)*	*575.62(3)*	*713.8(2)*
density (g/cm^3)		*6.535*	*6.539*	
Z		*2*		
Atom number		*7*		*2*
RF		*6.18*	*2.33*	*0.778*
RB		*10.2*	*4.75*	*1.95*
Rp		*9.46*	*7.91*	
Rwp		*13.6*	*11.1*	
cRp		*19.6*	*13.7*	
cRwp		*23.3*	*17.0*	

Table.2

Atomic coordinates, occupancy factors and thermal displacement parameters (Å2) of $NaPb_2CaSr(PO4)3$ 2nd Refinement.

atom	Wyckoff	Sym	x/a	y/b	z/c	B (Å²)	occupancy
Pb/Ca/Sr	6h	m	0.2563(2)	0.2540(2)	0.25	0.66(5)	1.90(2)/0.35(2)/0.75
Pb/Ca/Sr/Na	4f	3	0.6667	0.3333	0.4968(15)	1.17(6)	0.10(3)/0.65(4)/0.25/1
P	6h	m	0.3671(8)	0.4028(10)	0.75	1.26(8)	3
O(1)	6h	m	0.4706(7)	0.3203(10)	0.75	1.45(10)	3
O(2)	12i	1	0.2627(13)	0.3516(10)	0.5649(2)	1.45(10)	6
O(3)	6h	m	0.4836(8)	0.5916(11)	0.75	1.45(10)	3

Table 3

Selected interatomic distances in (Å) and O–P–O angles in (°) for NaPb2CaSr(PO4)3 2nd Refinements.

Atoms	Distance	Atoms	Distance
M(1)-O1	2.754(2)	M(2)-O1	2.572(7)
M(1)-O2	2.419(10)	M(2)-O1	2.571(7)
M(1)-O2	2.569(13)	M(2)-O1	2.572(7)
M(1)-O2	2.569(13)	M(2)-O2	2.804(10)
M(1)-O2	2.419(10)	M(2)-O2	2.803(9)
M(1)-O3	2.191(2)	M(2)-O2	2.803(14)
<M(1)-O>	2.487	M(2)-O3	2.602(7)
Atoms	Angle	M(2)-O3	2.603(7)
O2-P-O2	112.8(7)	M(2)-O3	2.602(7)
O1-P-O2	108.2(9)	<M(2)-O>	2.660
O1-P-O2	108.2(9)	P-O1	1.561(11)
O1-P-O3	108.6(5)	P-O2	1.580(10)
O2-P-O3	109.5(7)	P-O2	1.580(10)
O2-P-O3	109.5(7)	P-O3	1.595(8)
<O-P-O>	109.4	<P-O>	1.579

Fig.5 shows the small tunnel which corresponds to the mixed site M(2) occupied by mono and divalent cations. These cations are coordinated to nine oxygen anions belonging to six distinct tetrahedra; each polyhedron is linked to 3 PO_4^{3-} tetrahedra via corners and to three others via edges (Fig.5, M(2)). The hexagonal tunnel in the other site with a much larger section M(1) is occupied by 63.3% lead, 11.7% calcium and 25% strontium divalent cations. These cations are inserted in to six fold sites that constitute the walls of the tunnels, each polyhedron is linked to 4 PO_4^{3-} tetrahedra via corners and to one PO_4^{3-} via edge (Fig.5, M(1)). Mathew et al. [26] and Engel et al [27] showed in their work that the stabilization of the apatite structural type seems to be directly related to the presence of a minimum electronic density within its large tunnels. In the normal apatites these negative charges could be brought either by the Y^- (F^-, Cl^-, OH^-…) anions that occupy the large tunnels that encompass 6_3 axes. Whenever the Y^- anions are removed from the lattice, the apatite network collapses giving rise to a mixture of phases or to a new structural type, except in the cases where the host channels are occupied by cations having lone pairs such as Pb^{2+} or Bi^{3+}. This structural stabilization has been interpreted in terms of orientation of the lone pairs $6s^2$ of lead within the tunnels.

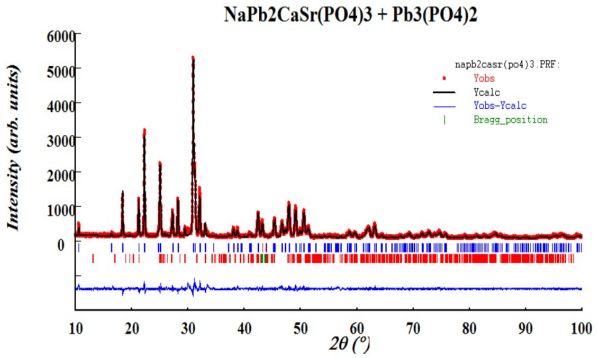

Fig.3. *Rietveld second refinements of the two phases of $NaPb_2CaSr(PO_4)_3$ and $Pb_3(PO_4)_2$. The upper symbols illustrate the observed data and the calculated pattern (solid line). The vertical markers show calculated positions of Bragg reflexions (R_{Bragg} = (4.75 and 1.95) %). The lower curve is the difference diagram.*

4. Vibrational spectra analysis and discussion

The Raman and IR spectra are analyzed with a view to study the influence of the sites M(1) and M(2), on the vibrational modes of phosphate groups. The factors that might be considered are the masse and the size of the cation.

$$\Gamma_{PO_4^{3-}} = 6A_g(\nu_1+\nu_2+2\nu_3+2\nu_4)+3E_{1g}(\nu_2+\nu_3+\nu_4)+6E_{2g}(\nu_1+\nu_2+2\nu_3+2\nu_4) + 3A_{u}(\nu_2+\nu_3+\nu_4)+6E_{1u}(\nu_1+\nu_2+2\nu_3+2\nu_4)$$

The formula of internal mode contribution of the PO_4^{3-} groups to the IR- and Raman-active vibrations where A_g, E_{1g} and E_{2g} normal modes are Raman-active, whereas A_u and E_{1u} normal modes are infrared active [13]. The internal modes from the tetrahedral phosphate ions, six per unit cell, can be deduced by the group factor analysis given in Table 4. For more details see Ref [9-11], note that we did not subtract the modes related to 2a sites (6_3 axes), which are vacant in the studied lead-phosphorus, vanadium and arsenic apatite structures.

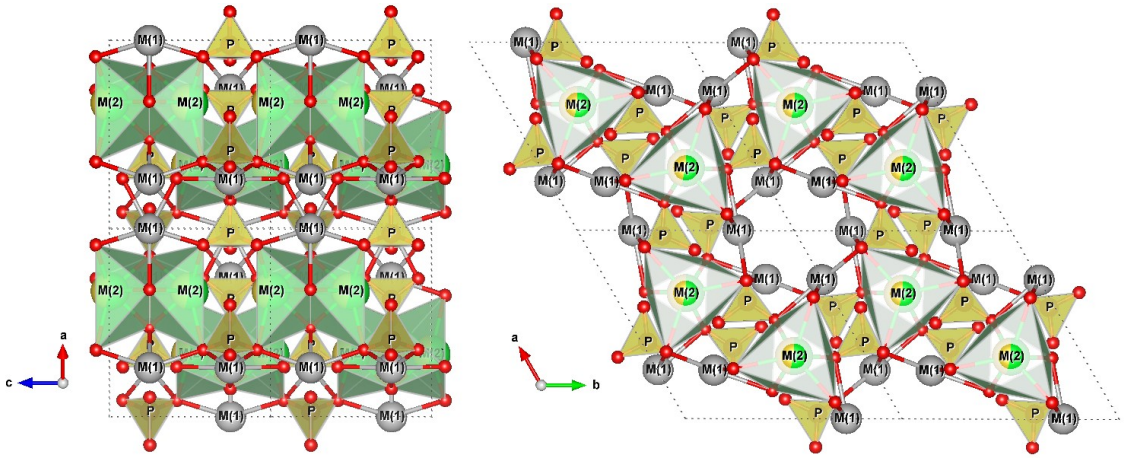

Fig.4. *Polyhedral view in the ab-plane of the crystal structure of $NaPb_2CaSr(PO_4)_3$.*

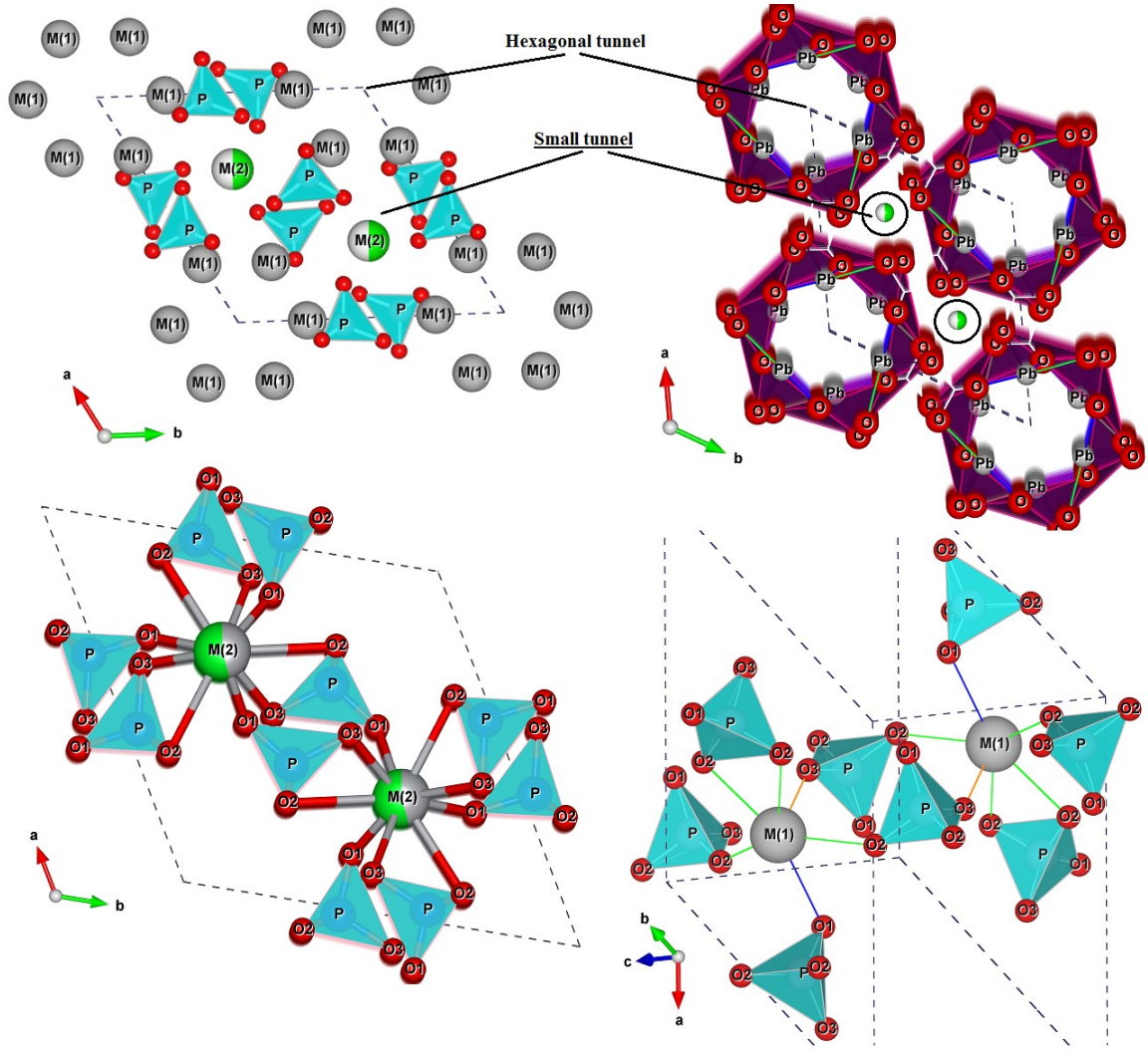

Fig.5*. Polyhedral view in the ab-plane of the crystal structure of $NaPb_2CaSr(PO_4)_3$ showing the tunnels. M(1) shows the site M(6h) of the big tunnel illustrating the metal and oxygen arrangement around (6h) sites connected to the $(PO_4)^{3-}$ tetrahedra. M(2) views the M(4f) prisme surrounded by the $(PO_4)^{3-}$ tetrahedra.*

Table 4 The factor group isomorphous with the space group C_{6h}^2 - $P6_3/m$ is C_{6h}.

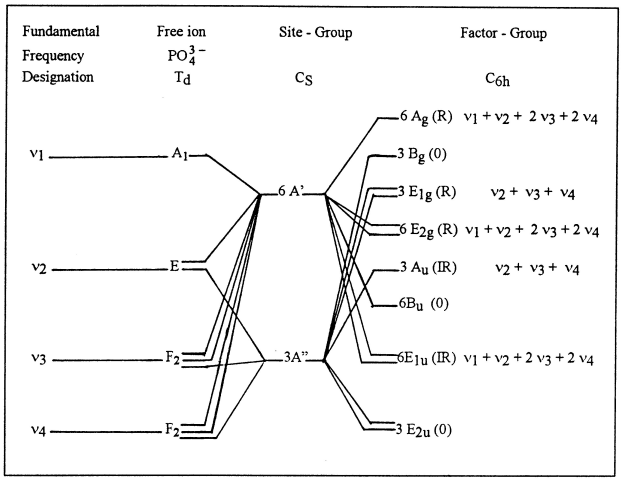

IR : active in IR , R : active in Raman , 0 : inactive

Fig.6 show the IR (a) and Raman (b) spectra of $NaPb_2CaSr(PO_4)_3$ recorded at ambient conditions. Since the specimens are polycrystalline powder, we cannot precisely assign the observed modes using a combination of the single-crystal orientation and the polarized Raman scattering.

The deconvolution of observed IR and Raman bands of synthetic $NaPb_2CaSr(PO_4)_3$ are presented in table.5. As shown, the observed Raman and IR modes can be classified into three general families of lattice vibrations: $Na^+/Pb^{2+}/Ca^{2+}/Sr^{2+}$-O (M(2)-O), $Pb^{2+}\backslash Ca^{2+}\backslash Sr^{2+}$-O (M(1)-O) external modes, as well as translational and rotational modes of PO_4 tetrahedra [9,16,17], these modes are observed at frequencies blew 400 cm^{-1}; a pattern of bands was observed in the 400-650 cm^{-1} region and is attributed to O-P-O bending vibrations [ν_2 (from 402 to 483 cm^{-1}) and ν_4 (from 552 to 597 cm^{-1})]; and the series of high frequency bands observed above 900 cm^{-1} are assigned to P-O stretching modes [ν_3 (from 1095 to 1100 cm^{-1}) and ν_1 (observed around 965 cm^{-1} to 1018 cm^{-1} as a strong band in the Raman spectra and as shoulder in the IR spectra)]. The bands observed in the infrared and Raman spectra of these compounds do not differ significantly from those observed for Ag lead apatite [11], lead phosphorus [8] and those of calcium hydroxyapatite whose factor group is C_{6h} [28,29].

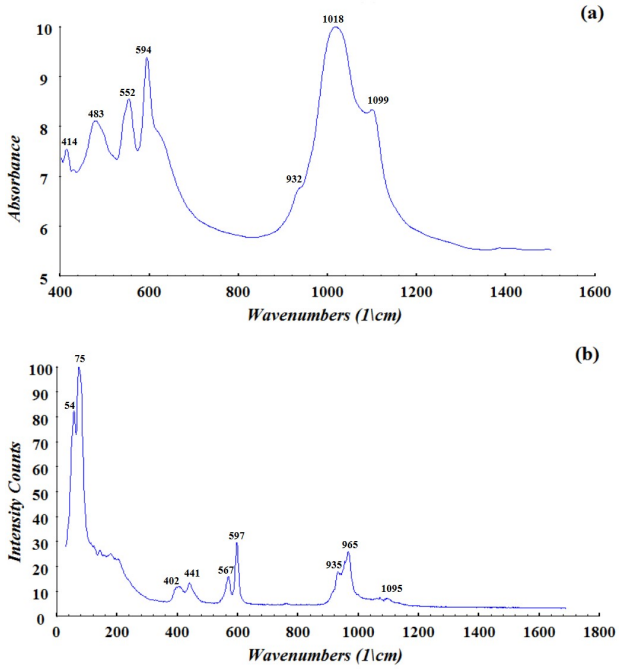

***Fig.6**. Infrared (a) and Raman (b) spectra of $NaPb_2CaSr(PO_4)_3$ at 293 K.*

Table5

The deconvolution of some of observed Raman and IR bands of synthetic $NaPb_2CaSr(PO_4)_3$

Modes	Lattice Modes		Bending Modes				Stretching Modes		
			ν_2		ν_4		ν_1		ν_3
Raman	54(s)	75(vs)	402(w)	441(m)	567(m)	597(s)	935(sh)	965(s)	1095(vm)
IR			414(w)	483(m)	552(s)	594(s)	932(sh)	1018(vs)	1099(s)

5. Partial elimination of toxic elements from phosphoric acid.

The OCP Company must overcome the increased demand for technical quality of phosphoric acid for various uses including the food industry and that of detergents, it is necessary for OCP to meet the new demands for phosphoric acid quality.

The main purpose of this test is to reduce the content of free sulfates, and others which are penalizing for the subsequent use of the acid such as (Cd, As, Ba, Mg ...) and must be eliminated. In 100 ml of PCA 54% in P_2O_5 unclarified and decanted, Morocco phosphorus sample, called pretreated acid, we added 100 mg of the lacunar apatite $NaPb_2CaSr(PO_4)_3$ with magnetic stirring (400rpm). The results of the test after filtration and the analysis by ICP are listed in the tables below. From the results illustrated in Table 6, $NaPb_2CaSr(PO_4)_3$ adsorbs partially all impurities except CaO molecules.

According to the results in Table 7, $NaPb_2CaSr(PO_4)_3$ adsorbs most of minor impurities with

high concentrations like for La and Sn, in medium content like for Ba, and in low contents such as for Cd, As, Ag, Li.... etc.

Table 6

Elimination percentages of the most abundant impurities in phosphoric acid.

Impurity (%)	Intreated PCA	Treated PCA	Yield in %
Al_2O_3	0.59	0.49	17
CaO	0.006	0.009	-
Fe_2O_3	0.34	0.31	9
K2O	0.148	0.123	17
MgO	1.69	1.54	9
Na_2O	0.069	0.052	25
SO_3	2.38	2.15	10

Table 7

Elimination percentages of minor impurities in phosphoric acid.

Minor impurities (mg/kg)	Intreated PCA	Treated PCA	Yield (%)
Cd	18.6	16.1	13
As	8.19	7.33	11
Cr	228	213	7
Cu	39	38	3
Mn	36	33	8
Ni	32	30	6
Sr	1.13	2.59	-
Ti	74	70	5
U	203	189	7
V	164	153	7
Zn	345	323	6
Ag	0.43	0.36	16
Ba	0.51	0.26	49
Be	1.48	1.36	8
Co	0.89	0.83	7
Er	2.33	2.16	7
Eu	0.099	0.095	4
La	0.02	0.00	100
Li	3.80	3.34	12
Mo	3.18	2.91	8
Pb	0.23	6.82	-
Sb	3.32	3.28	1
Sn	0.234	0.064	73
Th	5.02	4.88	3
Y	39	37	5
Zr	32	31	3

6. Conclusion

$NaPb_2CaSr(PO_4)_3$ lacunar apatite in the system of Na_2O–SrO–CaO–PbO–P_2O_5,was successfully synthesized by the solid-state reaction method. The compound was characterized by X-ray diffraction, Raman and infrared spectroscopies. Its structure has been determined by Rietveld method, adopting the space group $P6_3/m$ (No. 176), with a=b=9.6684(3)Å and c=7.1104(3)Å. The analysis shows that the M(2) sites are shared by four cations Ca, Sr, Pb and Na. While the M(1) are occupied by the Ca, Sr and Pb cations. The structure was described as built up from $[PO_4]^{3-}$ tetrahedra and $Pb^{2+}/Ca^{2+}/Sr^{2+}$ of six fold coordination cavities (6h positions), which delimit void hexagonal tunnels running along [0 0 1]. The tunnels are connected by cations of mixed sites (4f) half occupied by $Pb^{2+}/Ca^{2+}/Sr^{2+}$ and half by Na^+ mixed alkali cations.

The results of vibrational spectroscopy were in good agreements with the XRD measurements, the assignments of internal modes of $(PO_4)^{3-}$ tetrahedra have been made as well as factor group analysis for the symmetry $P6_3/m$.

An attempt to partially purify phosphoric acid has been done using our synthesized apatite. The results show a good sign of purification, we are looking forward to increase the yields to purify the acid.

Acknowledgement

The authors are grateful to the “Office Chérifien des Phosphates” in the Moroccan Kingdom (OCP group) and University Mohammed VI Polytechnic, the University Hassan 1st for its support and the Swedish Research Council for the financial grant SRL(MENA) # 348- 2014-4287.

References

[1] St. Náray-Szabó, Zeitschrift für Kristallographie 75 (1930) 387-398,

[2] M. Pasero, A.R. Kampf, C. Ferraris, I.V. Pekov, Rakovan, T.J. White, European Journal of Mineralogy 22(2) (2010) 163-179.

[3] J.C. Elliott, Structure and chemistry of the apatites and other calcium orthophosphates, in: Studies in Inorganic Chemistry, Vol. 18. Elsevier, Amsterdam, 1994.

[4] D. McConnell, Apatite: its crystal chemistry, mineralogy, utilization, and geologic and biologic occurrences, Applied mineralogy 5, Springer-Verlag, New York/ Vienne, 1973.

[5] G. Wright, G. Montel, Comptes rendus de l'Académie des Sciences Paris, 268C (1969) 2077-2080.

[6] R.Z. LeGeros, M.H. Taheri, G.B. Quirolgico, J.P, Legeros, Formation and stability of apatites: effects of some cationic substituents, in: Proc 2nd International Congress on Phosphorus Compounds, Boston. pp. 89–103.

[7] M. El Koumiri, S. Oishi, S. Sato, L. El Ammari, B. Elouadi. Materials Research Bulletin 35 (2000) 503-513.

[8] B. Hamdi, H. El Feki, J.M. Savariault, A. Ben Salah. Materials Research Bulletin 42 (2007) 299-311.

[9] M. Azrour, M. Azdouz, B. Manoun, R. Essehli, S. Benmokhtar, L. Bih, L. El Ammari, A. Ezzahi, A. Ider, A. Ait Hou, Journal of Physics and Chemistry of Solids 72 (2011) 1199-1205.
[10] M. Azdouz, B. Manoun, M. Azrour, L. Bih, L. ElAmmari, S. Benmokhtar, P. Lazor, Journal of Molecular Structure 963 (2010) 258-266.
[11] B. Manoun, M. Azdouz, M. Azrour, R. Essehli, S. Benmokhtar, L. ElAmmari, A. Ezzahi, A. Ider, P. Lazor, Journal of Molecular Structure 986 (2011) 1-9.
[12] M. Quarton, M.T. Oumba, W. Freundlich, A.W. Kolsi, Materials Research Bulletin 19 (1984) 1063-1068.
[13] R. Ternane, M. Ferid, M. Trabelsi-Ayadi, B. Piriou, Spectrochimica Acta A (55) (1999) 1793- 1797.
[14] T. Naddari, H. El Feki, J.M. Savariault, P. Salles, A. Ben Salah, Solid State Ionics 158 (2003) 157-166.
[15] Z. Elouear, J. Bouzid, N. Boujelben, M. Feki, F. Jamoussi, A. Montiel, Jornal of Hazardous Materials 156 (2008) 412–420.
[16] S. Lahrich, B. Manoun, M.A. El Mhammedi, Materials Research Bulletin 59 (2014) 349–357.
[17] S. Lahrich, B. Manoun, M.A. El Mhammedi, Talanta 149(1) (2016) 158-167.
[18] J. Rodriguez-Carvajal, FULLPROF: A Program for Rietveld Refinement and Pattern Matching Analysis", Abstracts of the Satellite Meeting on Powder Diffraction of the XV Congress of the IUCr, Toulouse, France, 1990, p. 127.
[19] H. Bih, L. Bih, B. Manoun, M. Azdouz, S. Benmokhtar, P. Lazor, Journal of Molecular Structure 936 (2009) 147–155.
[20] A. Boultif, D. Louër, Journal of Applied Crystallography 24 (1991) 987-993.
[21] T. Roisnel, J. Rodriguez-Carvajal, Materials Science Forum 378–381 (2001) 118-123.
[22] S. Lahrich, M.A. Elmhammedi, B. Manoun, Y. Tamraoui, F. Mirinioui, M. Azrour, P. Lazor, Spectrochimica Acta A 145 (2015) 493-499.
[23] G. Caglioti, A. Paoletti, F.P. Ricci, Nuclear Instruments and Methods 3 (1958) 223-228.
[24] T. Degen, M. Sadki, E. Bron, U. König, G. Nénert, Powder Diffraction 29 (2014) S13-S18.
[25] C. Joffrin, J.P. Benoit, L. Deschamps, M. Lambert, Journal de Physique France 38 (1977) 205-213.
[26] M. Mathew, W.E. Brown, M. Austin, T. Negas, Journal of Solid State Chemistry 35 (1980) 69-76.
[27] G. Engel, W. Gotz, R. Eger, Z. Anorg. allgemeine Chemie 449 (1979) 127-134.
[28] B.O. Fowler, Inorganic Chemistry 13 (1974) 194-207.
[29] K.C. Blakeslee, R.A. Condrate, Journal of the American Ceramic Society 54 (1971) 559-563.